http://dx.doi.org/10.21577/0103-5053.20180195

J. Braz. Chem. Soc., Vol. 30, No. 4, 744-751, 2019
Printed in Brazil - ©2019 Sociedade Brasileira de Química

Article

Cr^{3+} Doped Al_2O_3 Obtained by Non-Hydrolytic Sol-Gel Methodology

José M. A. Caiut,[,a] Nolwen Floch,[b] Younès Messaddeq,[b] Omar J. de Lima,[c] Lucas A. Rocha,[c] Katia J. Ciuffi,[c] Eduardo J. Nassar,*[,c] Geraldo R. Friedermann[d] and Sidney J. L. Ribeiro[b]*

[a]*Departamento de Química, Faculdade de Filosofia, Ciências e Letras de Ribeirão Preto (FFCLRP), Universidade de São Paulo (USP), 14040-901 Ribeirão Preto-SP, Brazil*

[b]*Instituto de Química, Universidade Estadual Paulista (Unesp), 14800-900 Araraquara-SP, Brazil*

[c]*Universidade de Franca (UNIFRAN), 14404-600 Franca-SP, Brazil*

[d]*Departamento de Química, Universidade Federal do Paraná (UFPR), 81531-980 Curitiba-PR, Brazil*

This paper reports the synthesis and characterization of Cr^{3+}-doped alumina by the sol-gel non-hydrolytic methodology. The resulting sample was treated at different temperatures. X-ray diffraction revealed that the ruby phase emerged in the sample treated at 1100 °C, which was later confirmed by absorption bands correspondent to Cr^{3+} ions allowed transitions at $^4A_2 \rightarrow {}^4T_1$, $^4T_2$, and forbidden at $^4A_2 \rightarrow {}^2T_1$, ^2E, observed by diffuse reflectance UV-Vis. The luminescence spectroscopy showed the intensity band at 694 nm in red region, characterized of the Cr^{3+} ion. The peaks at 702 and 705 nm correspond to N_1 and N_2 lines, respectively, which arose from the second and fourth nearest-neighbor exchange-coupled pairs of chromium(III) ion, respectively, ascribed to high chromium(III) concentration. The Cr^{3+} cluster formation was observed in electron paramagnetic resonance signal as discussed in this work. Nuclear magnetic resonance evidenced that the ^{27}Al symmetry changed in the samples treated between 900 and 1100 °C.

Keywords: ruby, EPR, NMR, sol-gel, luminescence

Introduction

Several matrices can be used as hosts for chromium(III) ions, e.g., $Be_3Al_2(SiO_3)_6:Cr^{3+}$,[1,2] $LiCaAlF_6:Cr^{3+}$,[3] $LiSrAlF_6:Cr^{3+}$,[4,5] $MgGa_2O_4:Cr^{3+}$,[6] and $MgAl_2O_4:Cr^{3+}$,[7] for further application as solid state lasers. Emission wavelength and emission efficiency depend on the host.[1-7] Ruby is a mineral species consisting of chromium(III) ions supported on α-alumina. This system presents several important technological applications, such as laser hosts, sensors of the pressure and temperature, and others.[8,9] The literature demonstrated the laser action of the ruby for the first time, performed the basic research that led to the invention of laser and maser devices.[10]

The particular sensitivity of the luminescence R lines to changes in pressure and temperature is important for sensor design.[11-13] Chromium(III) spectroscopy has been interpreted by ligand field theory. This ion has strong visible absorption bands due to electronic excitation from the ground state $^4A_2$ to states $^4T_1$ and $^4T_2$. Non-radiative transition from these states to state ^2E rapidly takes place, and electron fall back from ^2E to the ground state is followed by the characteristic luminescence at 695 nm.[14,15]

The processes used for preparation of mixed metal oxide systems need high temperature, pressure, several kinds of reagent, and severe synthesis conditions. The Verneuil process has been used to produce synthetic ruby since 1902. This process consists of flame fusion.[16] Other processes such as hydrothermal synthesis and fusion have also been employed.[17,18] More recently, the sol-gel methodology has been used to dope alumina with chromium(III) ions.[19,20] The advantage of the non-hydrolytic sol-gel process is due to using basic reagent (salts), and the reaction may be carried out in a sealed tube at temperatures around 110 °C using inert atmosphere.

The sol-gel non-hydrolytic methodology has been successfully employed to prepare doped matrices for several applications. Examples of such matrices include yttrium aluminum garnet (YAG),[21-23] $GdCaAl_3O_7$,[24,25] YVO_4,[26-30] $SrWO_4:Eu^{3+}$,[31,32] $Nb_2O_5:La^{3+}Eu^{3+}$,[33] $GdNbO_4:Eu^{3+}$,[34] indium

*e-mail: caiut@ffclrp.usp.br; eduardo.nassar@unifran.edu.br

tin oxide (ITO),[35] Nb-aluminum oxide,[36] iron-aluminum,[37] glass ionomer,[38,39] aluminum doped with cobalt,[40] Eu^{3+}-doped alumina matrix,[41] and porphyrin-doped alumina matrix.[42] This methodology is based on the condensation between a metallic halide (M–X) and a metallic alkoxide (M'–OR), to yield an oxide (M–O–M').[43]

In this work, we prepared alumina doped with chromium(III) ions by the sol-gel non-hydrolytic methodology to obtain the ruby phase. We investigated the influence of the thermal treatment temperature on the prepared material by photoluminescence (PL), X-ray diffraction (XRD), nuclear magnetic resonance (NMR), and electron paramagnetic resonance (EPR) measurements.

Experimental

The desired material was synthesized by means of the non-hydrolytic sol-gel method described by Acosta *et al.*[44] and modified by us.[41] The Cr^{3+}-doped alumina sols were prepared by reflux of 2.0 g (0.015 mol) of aluminum chloride ($AlCl_3$) and 25.0 mL (0.18 mol) of di-isopropyl ether (*i*-Pr_2O) in 40.0 mL of dry dichloromethane (DCM) and 20.0 mL of absolute ethanol at 110 °C, under argon atmosphere. Chromium(III) chloride was added to obtain doping at 2.0% molar ratio (Cr^{3+}:Al^{3+}). The condenser was connected to a thermostatic bath at –5 °C. The mixture was kept under reflux for 270 min. The obtained gel was cooled and aged at room temperature for 20 h. Next, the sol was concentrated under vacuum. The powder structure was investigated after thermal treatment at 900 and 1100 °C.

Samples were characterized by XRD on a Siemens D 5000 diffractometer operating with Cu radiation (0.05° s^{-1}). PL spectra of powder samples were recorded on a SPEX-fluorog fluorometer model F212I equipped with double monochromators for excitation and emission and a 450 W xenon lamp. For powder samples, the aluminum site was analyzed by ^{27}Al NMR on a Bruker Avance III 400WB HD spectrometer with Larmor frequency of 59.5 MHz for ^{27}Al. EPR measurements of the chromium(III) ion in the powder samples subjected to thermal treatment were performed on a Bruker ESP 300E spectrometer at the X-band (ca 9.5 GHz), at 293 or 77 K; liquid N_2 was used. The powder samples were analyzed by diffuse reflectance UV-Vis spectroscopy on a CARY spectrophotometer (5000 UV-VIS-NIR) in the 200-800 nm range.

Results and Discussion

Chromium(III) insertion into alumina matrices, like ruby, was achieved by a sol-gel non-hydrolytic methodology. This method is based on aluminum halide condensation with ether: O–R bonds are cleaved, and alkyl halides emerge. Alumina gelation originates from alkoxide-halide non-hydrolytic condensation, and an alkyl halide is released.

The non-hydrolytic sol-gel route is based on condensation reaction between alkoxide (M–OR) and halide (M–X), the alkoxide is obtained *in situ* by reaction between an oxygen donor such as ether (R–O–R) with halide (Scheme 1). The probable mechanism for the formation of Al_2O_3 matrix doped with Cr^{3+} can be represented by Scheme 1.

The mechanism for the formation of Al_2O_3 matrix doped with Cr^{3+} can be represented by the Scheme 2, and can occur by three different routes. The ligand can be substituted by nucleophilic bimolecular S_{N2} (route 1), S_{N2} combined (route 2), and through the nucleophilic unimolecular S_{N1} (route 3).[46-48]

The non-hydrolytic alumina remained amorphous up to 900 °C, but samples treated at 1100 °C displayed a crystalline phase, as evidenced by the XRD pattern, which revealed corundum aluminum oxide formation (Al_2O_3 powder diffraction file (PDF) No. 43-1484). Figures 1a and 1b depict the XRD patterns of the samples treated at 900 and 1100 °C, respectively.

The XRD patterns evidenced formation of ruby phases at 1100 °C, as indicated by the peaks at 2θ = 35.07, 43.14, and 57.39°. These peaks corresponded to PDF No. 43-1484, which can be indexed to the rhombohedral form of space group R32/c (No. 167). The crystallinity degree of the samples can be evaluated by XRD; the low value at full width half maximum (FWHM) of the peak is an indicative of high crystallinity. Ribeiro and Prado[49] observed values ranging from 0.10 to 0.14, very close to those observed for monocrystals of silicon and crystalline quartz. The FWHM of some of the diffraction peaks of the ruby synthesized in this work were between 0.16 and 0.34° and can be attributed to a high crystallinity degree. Table 1 lists the normalized intensities of the crystalline plane with the respective Miller indices as well as the interplanar distance.

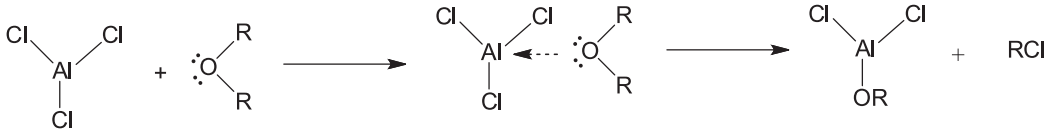

Scheme 1. Mechanism of the alkoxide formation.

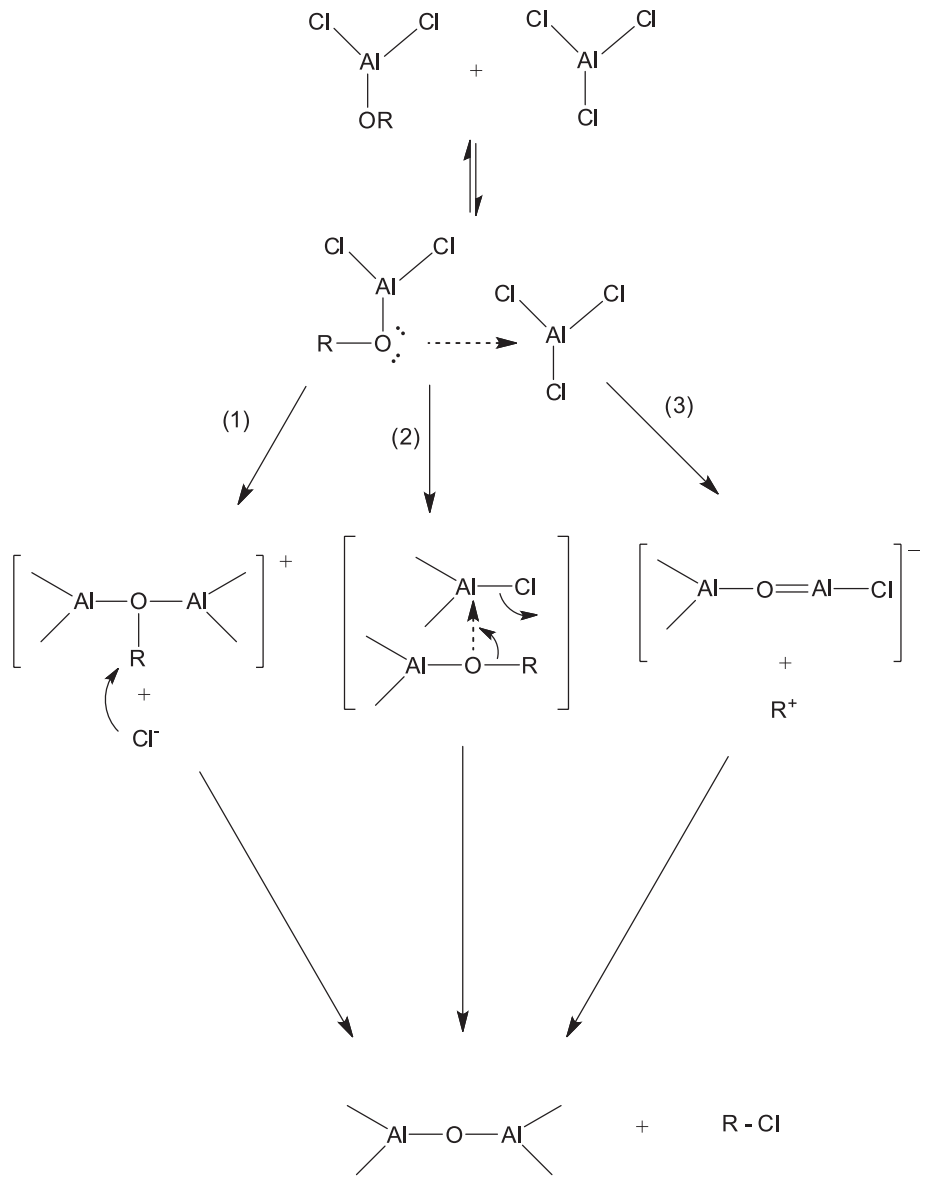

Scheme 2. The non-hydrolytic sol-gel methodology mechanism (adapted from reference 45).

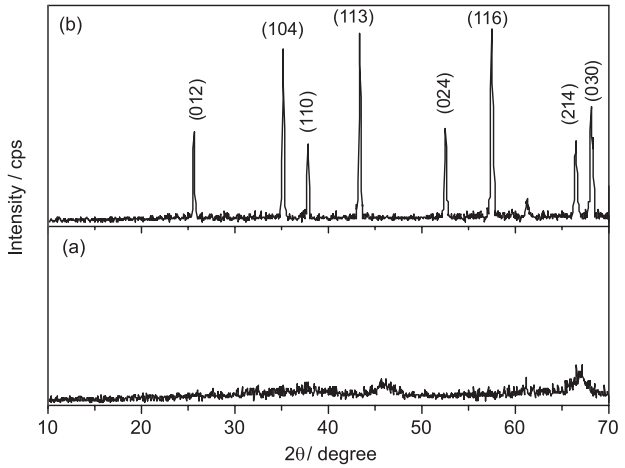

Figure 1. XRD patterns of Cr^{3+}-doped alumina powder samples treated at (a) 900 and (b) 1100 °C.

Comparison between the experimental and literature[50] data showed very similar results, which indicated that the sol-gel non-hydrolytic methodology afforded synthetic ruby (α-Al_2O_3). This result will be later confirmed by other techniques.

Figure 2 presents the ^{27}Al NMR spectrum of the powder samples treated at 900 and 1100 °C. When Al atoms are in tetrahedral coordination (Al^{IV}), their chemical shifts vary from 55 to 80 ppm, whereas chemical shifts ranging from –10 to 10 ppm correspond to octahedral coordination (Al^{VI}).[39,44,46,51-56] The resonance spectra showed that the ^{27}Al symmetry site changed depending on temperature. Cr^{3+}-doped alumina treated at 900 °C displayed signals at 6.8 and 65.8 ppm, which corresponded to hexacoordinated (Al^{VI}) and tetracoordinated (Al^{IV}) coordination, respectively.

Table 1. 2θ angles, interplanar distance, Miller indices, and relative intensity obtained from the XRD patterns of the prepared Cr^{3+}-doped alumina powder samples as compared to literature data

2θ / degree	$2\theta_{lit}$ / degree	d / Å	d_{lit} / Å	*hkl*	I / I_0	$(I / I_0)_{lit}$
25.57	25.43	3.479	3.499	0 1 2	47	60
35.07	34.94	2.556	2.565	1 0 4	90	92
37.68	37.55	2.384	2.393	1 1 0	40	46
43.14	43.09	2.094	2.097	1 1 3	96	88
52.40	52.22	1.744	1.749	0 2 4	47	50
57.39	57.14	1.604	1.610	1 1 6	100	100
66.41	66.08	1.406	1.412	2 1 4	41	42
68.07	67.75	1.375	1.382	3 0 0	48	30

d: interplanar distance; *hkl*: Miller index; I / I_0: relative intensity. The subscript lit refers to literature data (PDF 43-1484).

The sample treated at 1100 °C presented only a signal at 11.9 ppm, which indicated that ^{27}Al occupied an octahedral symmetry site. The ruby structure only contains aluminum octahedral symmetry sites, so the ^{27}Al NMR spectra confirmed the ruby phase in the sample treated at 1100 °C.

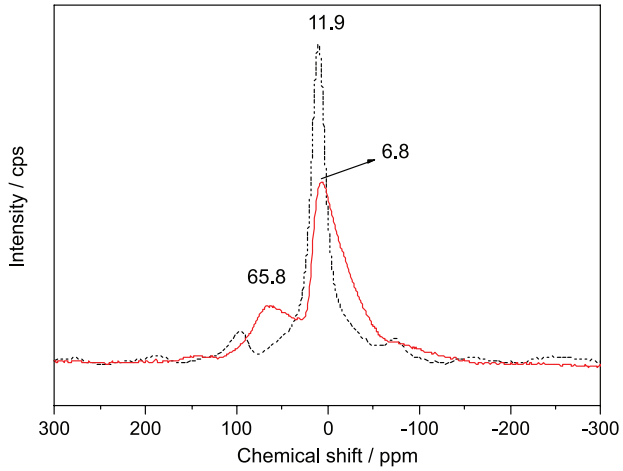

Figure 2. ^{27}Al NMR spectra of the Cr^{3+}-doped alumina powder samples treated at 900 °C (red solid line) and 1100 °C (black dashed line).

The EPR study helped to characterize the electronic environment of chromium(III) ions in Cr^{3+}-doped alumina prepared by sol-gel non-hydrolytic methodology. Figure 3 contains the EPR spectra recorded for the samples treated at 900 and 1100 °C. The EPR spectrum of the sample treated at 900 °C presented a signal with g_{iso} = 1.97 and a broad line with g = 2.65, characteristic of Cr^{3+}-doped γ-alumina and chromium(III) ions in phases β and δ, respectively. The chromium ions are randomly distributed into the matrix, the distance between Cr^{3+}-Cr^{3+} decreases with increasing concentration, leading to formation of Cr^{3+} clusters. Confirmation of the clusters formation can be made through EPR measurements. Patra *et al.*[50] observed the EPR at g = 1.99 for ca. 3400 G ascribed to Cr^{3+} clusters. In this work, the EPR signal appears at g = 1.97 for 3451 G, confirming the Cr^{3+} clusters formation. This signal disappeared in the EPR spectrum of the sample treated at 1100 °C, which confirmed octahedral symmetry. The EPR spectra showed a signal with g ca. 3.45, which suggested the presence of chromium(III) ions in distorted octahedral symmetry. This is the case of the ruby structure, where small Al^{3+} ions were replaced with larger Cr^{3+} ions, and the size difference distorted the corundum lattice.

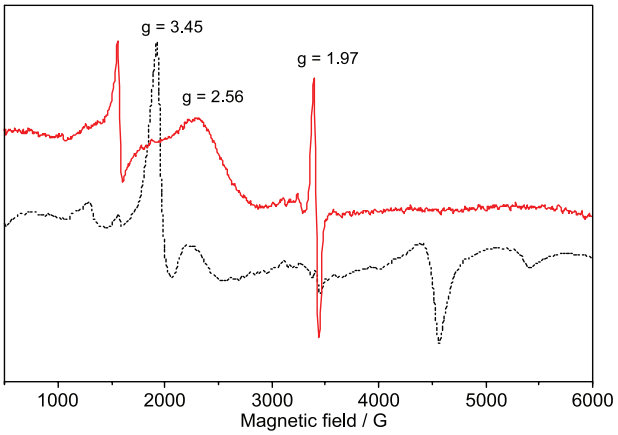

Figure 3. EPR spectra of the Cr^{3+}-doped alumina powder samples treated at 900 °C (red solid line) and 1100 °C (black dashed line).

Figure 4 shows the diffuse reflectance UV-Vis spectra of the powder sample treated at 1100 °C, with absorption bands due to two spin-allowed transitions, $^4A_2 \rightarrow {}^4T_1$ (405 nm) and $^4A_2 \rightarrow {}^4T_2$ (562 nm), and spin-forbidden bands between 650 and 710 nm. In that case, the transitions from excited levels $^2T_1$ and ^2E to ground state $^4A_2$ were shown by a group of narrowed bands in the spectrum, and it were resulted from the spin-orbit interaction and trigonal crystal-field distortion effects on these levels. Finally, the spectrum showed the R and N lines at high and low energy, respectively. And the intensity ratio of N line to R line was consequence of the

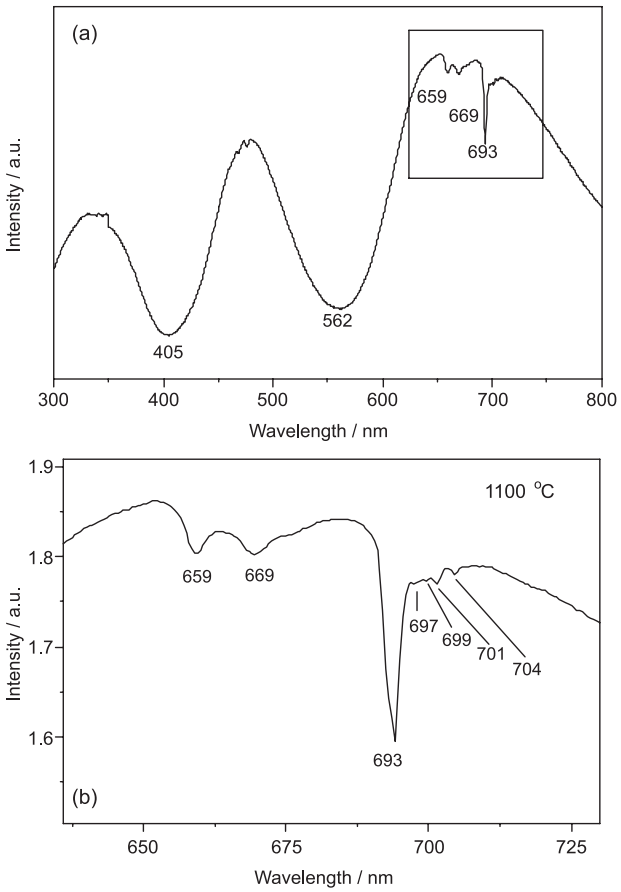

Figure 4. (a) Diffuse reflectance UV-Vis spectrum of the Cr^{3+}-doped alumina powder sample treated at 1100 °C; (b) magnification of selected area.

chromium concentration, as shown by Powell.[51] The noticed baseline change after 750 nm was not by matrix absorption, but it was a baseline artifact resulting from wavelength lamp exchange in the equipment.

Figure 5 shows the Tanabe-Sugano diagram[57] of the d^3 energy level configuration of octahedral symmetry and the absorption spectrum of the Cr^{3+}-doped alumina powder sample treated at 1100 °C.

The narrow bands between 650 and 710 nm were ascribed to the spin-forbidden transitions $^2T_1 \rightarrow {}^4A_2$ and $^2E \rightarrow {}^4A_2$. The crystal field parameter (Dq) and Racah (B) parameters were calculated from the excitation bands. Dq and B were determined from the location of the bands corresponding to transitions $^4A_2 \rightarrow {}^4T_2$ and $^4A_2 \rightarrow {}^4T_1$, respectively.[15] Dq was 1773 cm^{-1}, B was 645 cm^{-1}, and Dq / B was 2.75, which agreed with values obtained for other systems with octahedral chromium(III) ions.[6,7,58,59]

Excitation spectra were recorded by fixing the emission wavelength at 694 nm (Figure 6). The spectra of the Cr^{3+}-doped alumina samples treated at 1100 °C displayed broad bands at 405 and 562 nm, which corresponded to spin-allowed transitions from the ground state $^4A_2$ to the excited states $^4T_2$ and $^4T_1$, respectively.[19] The excitation spectra indicated the octahedral symmetry of the chromium(III) ion replacing Al^{3+} in the alumina matrix.

The small band at 475 nm (Figure 6) can be ascribed to spin forbidden transition at $^4A_2 \rightarrow {}^2T_2$. The low intense band

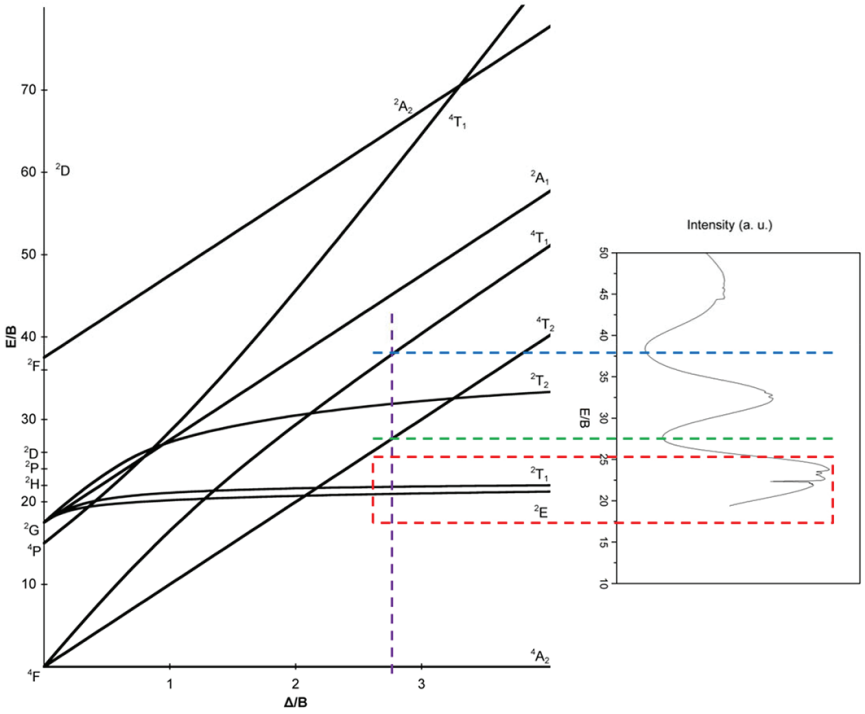

Figure 5. Tanabe-Sugano diagram of the d^3 energy level configuration of octahedral symmetry and absorption spectrum of the Cr^{3+}-doped alumina powder sample treated at 1100 °C.

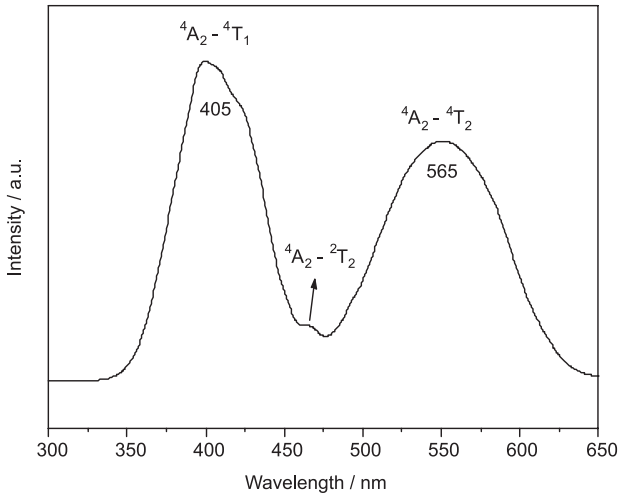

Figure 6. Excitation spectra of Cr^{3+}-doped alumina powder sample treated at 1100 °C. λ_{em} = 694 nm.

attributed at the $^4A_2$ and $^2T_2$ was a spin forbidden transition.

Figure 7 illustrates the emission spectra of Cr^{3+}-doped alumina powder sample treated at 1100 °C in two different excitation lines, 405 nm (Figure 7a), and 565 nm (Figure 7b). The emission spectra of the Cr^{3+}-doped alumina powder were recorded at room temperature. The spectra contained the well-known sharp R lines at 694 nm, attributed to transition $^2E \rightarrow {}^4A_2$ of single Cr^{3+} ions in ruby. The emission spectra indicated that chromium(III) ions occupied octahedral sites.[19] The peak around 670 nm in the spectrum of the powder sample referred to the lines of transition $^2T_1 \rightarrow {}^4A_2$.[47] Jamison and Imbusch[53] ascribed the peaks at 702 and 705 nm to N_1 and N_2 lines, respectively, which arose from the second and fourth nearest-neighbor exchange-coupled pairs of chromium(III) ions, respectively, due to high chromium(III) concentration. The Cr^{3+} cluster formation was observed in EPR signal as discussed in this work.

The broad band above 705 nm, resulting from the location of Cr pairs, was also observed in literature.[60,61] The bands at 701 and 705 nm are ascribed to N_2 and N_1 lines of the Cr^{3+}, respectively, with some overlap with the vibronic line peaks at 707 and 714 nm.[62,63] The vibronic band at 714 nm is more intense when excited at 405 nm; this fact explained the resolution and intensity of the emission spectra, the vibration mode acts to disable the excited state.

Conclusions

The sol-gel non-hydrolytic route is an important methodology to produce multifunctional materials. Cr^{3+}-doped alumina powder treated at 1100 °C displayed the ruby phase. The XRD, PL, and diffuse reflectance UV-Vis analyses showed that the chromium(III) ion was incorporated into the alumina matrix and occupied a distorted octahedral symmetry site after it substituted Al^{3+} in the matrix. ^{27}Al NMR and EPR characterization confirmed this substitution, which generated the ruby structure.

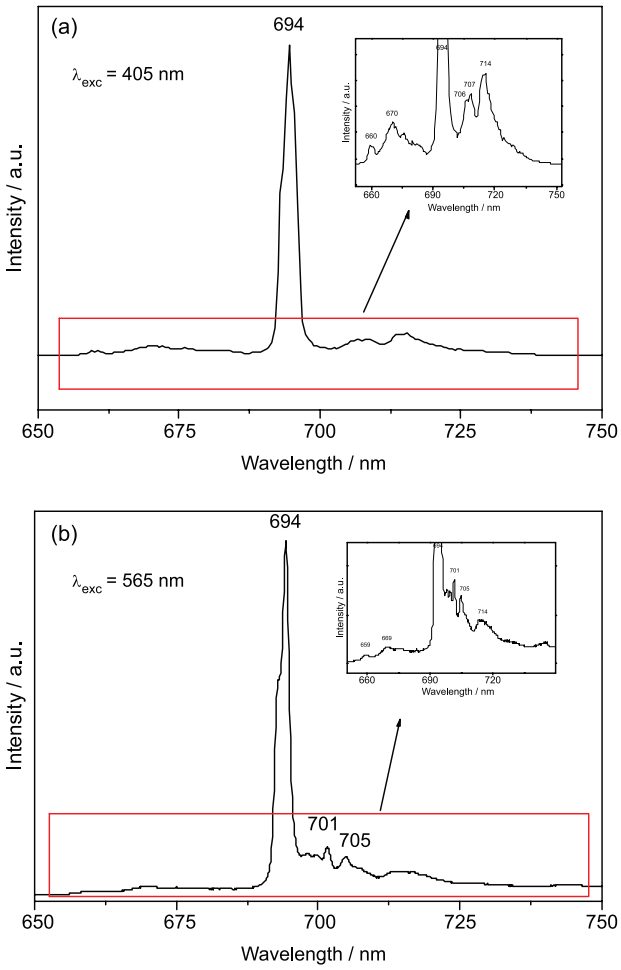

Figure 7. Emission spectra of Cr^{3+}-doped alumina powder sample treated at 1100 °C. λ_{exc} = 405 nm (a), and λ_{exc} = 565 nm (b).

Acknowledgments

The authors acknowledge CNPq and CAPES (Brazilian research funding agencies) and the São Paulo Research Foundation (FAPESP, Brazil, Proc. 2002/06560-3) for support of this work. Cynthia Maria de Campos Prado Manso is acknowledged for careful revision of the text in English.

References

1. Shand, M. L.; Lai, S. T.; *IEEE J. Quantum Electron*. **1984**, *20*, 105.
2. Lai, S. T.; *J. Opt. Soc. Am. B* **1987**, *4*, 1286.
3. Payne, S. A.; Chase, L. L.; Newkirk, H. W.; *IEEE J. Quantum Electron.* **1988**, *24*, 2243.

4. Stalder, M.; Chat, B. H. T.; Bass, M.; *Appl. Phys. Lett.* **1991**, *58*, 216.
5. Payne, S. A.; Chase, L. L.; Smith, L. K.; *J. Appl. Phys.* **1989**, *66*, 1051.
6. Garapon, C.; Brenier, A.; Moncorgé, R.; *Opt. Mater.* **1998**, *10*, 177.
7. Deren, P. J.; Malinowiski, M.; Strek, W.; *J. Lumin.* **1996**, *68*, 91.
8. Fahlman, B. D.; Barron, A. R.; *Chem. Vap. Deposition* **2001**, *7*, 62.
9. Rousseau, D. L.; *J. Chem. Educ*. **1996**, *43*, 566.
10. Shampo, M. A.; Kyle, R. A.; Steensma, D. P.; *Mayo Clin. Proc.* **2011**, *86*, e33.
11. Gibson, U.; Chernuschenko, M.; *Opt. Express* **1999**, *4*, 443.
12. Nicol, M.; Yen, J.; *J. Appl. Phys*. **1992**, *72*, 5535.
13. Clarke, D. R.; Wen, Q.; Yu, N.; Nastasi, M.; *Appl. Phys. Lett.* **1995**, *66*, 293.
14. Huang, T. H.; Hsu, C. C.; Kuo, C. T.; Fuh, A. Y. G.; *J. Appl. Phys.* **1994**, *75*, 3599.
15. Henderson, B.; Imbusch, G. F.; *Optical Spectroscopy of Inorganic Solids*, 1st ed.; Clarendon Press: Oxford, 1989.
16. Arivuoli, D. In *Encyclopedia of Materials: Science and Technology*, 2nd ed.; Buschow, K. H. J.; Cahn, R. W.; Flemings, M. C.; Ilschner, B.; Kramer, E. J.; Mahajan, S.; Veyssière, P., eds.; Elsevier: Amsterdam, 2001, p. 7854.
17. Liu, D.; Zhu, Z.; Liu, H.; Zhang, Z.; Zhang, Y.; Li, G.; *Mater. Res. Bull.* **2012**, *47*, 2332.
18. Silva, G.; Prado, R. J.; *Quim. Nova* **2010**, *33*, 1104.
19. Fujita, K.; Tokudome, Y.; Nakanishi, K.; Miura, K.; Hirao, K.; *J. Non-Cryst. Solids* **2008**, *354*, 659.
20. Eckert, C.; Pflitsch, C.; Atakan, B.; *Prog. Org. Coat.* **2010**, *67*, 116.
21. Pereira, P. F. S.; Matos, M. G.; Ferreira, C. M. A.; de Faria, E. H.; Calefi, P. S.; Rocha, L. A.; Ciuffi, K. J.; Nassar, E. J.; *J. Lumin.* **2014**, *146*, 394.
22. Pereira, P. F. S.; Matos, M. G.; Ávila, L. R.; Nassor, E. C. O.; Cestari, A.; Ciuffi, K. J.; Calefi, P. S.; Nassar, E. J.; *J. Lumin.* **2010**, *130*, 488**.**
23. Nassar, E. J.; Ávila, L. R.; Pereira, P. F. S.; Melo, C.; de Lima, O. J.; Ciuffi, K. J.; Carlos, L. D.; *J. Lumin.* **2005**, *111*, 159.
24. Matos, M. G.; Calefi, P. S.; Ciuffi, K. J.; Nassar, E. J.; *Inorg. Chim. Acta* **2011**, *375*, 63.
25. Matos, M. G.; Pereira, P. F. S.; Calefi, P. S.; Ciuffi, K. J.; Nassar, E. J.; *J. Lumin.* **2009**, *129*, 1120.
26. Miura, B. A.; Ferreira, N. H.; Oliveira, P. F.; de Faria, E. H.; Tavares, D. C.; Rocha, L. A.; Ciuffi, K. J.; Nassar, E. J.; *J. Lumin.* **2015**, *159*, 93.
27. Saltarelli, M.; Matos, M. G.; de Faria, E. H.; Ciuffi, K. J.; Rocha, L. A.; Nassar, E. J.; *J. Sol-Gel Sci. Technol.* **2015**, *73*, 283.
28. Matos, M. G.; de Faria, E. H.; Rocha, L. A.; Calefi, P. S.; Ciuffi, K. J.; Nassar, E. J.; Sarmento, V. H. V.; *J. Lumin.* **2014**, *147*, 190.
29. Matos, M. G.; Rocha, L. A.; Nassar, E. J.; Verelst, M.; *Opt. Mater.* **2016**, *62*, 12.
30. Saltarelli, M.; Luz, P. P.; Matos, M. G.; de Faria, E. H.; Ciuffi, K. J.; Calefi, P. S.; Rocha, L. A.; Nassar, E. J.; *J. Fluoresc.* **2012**, *22*, 899.
31. Pereira, P. F. S.; de Moura, A. P.; Nogueira, I. C.; Lima, M. V.; Longo, E.; de Souza Filho, P. C.; Serra, O. A.; Nassar, E. J.; Rosa, I. L. V.; *J. Alloys Compd*. **2012**, *526*, 11.
32. Pereira, P. F. S.; Nogueira, I. C.; Longo, E.; Nassar, E. J.; Rosa, I. L. V.; Cavalcante, L. S.; *J. Rare Earths* **2015**, *33*, 113.
33. Matias, C. R.; Nassar, E. J.; Verelst, M.; Rocha, L. A.; *J. Braz. Chem. Soc.* **2015**, *26*, 2558.
34. Oliveira, L.; Moscardini, S. B.; Nassar, E. J.; Molina, E. F.; Verelst, M.; Rocha, L. A.; *Nanotechnology* **2018**, *29*, 235204.
35. Silva, G. M.; de Faria, E. H.; Nassar, E. J.; Ciuffi, K. J.; Calefi, P. S.; *Quim. Nova* **2012**, *35*, 473.
36. Alfenas, C. S.; Ricci, G. P.; de Faria, E. H.; Saltarelli, M.; de Lima, O. J.; da Rocha, Z. N.; Nassar, E. J.; Calefi, P. S.; Montanari, L. B.; Martins, C. H. G.; Ciuffi, K. J.; *J. Mol. Catal. A: Chem.* **2011**, *338*, 65.
37. Ricci, G. P.; Rocha, Z. N.; Nakagaki, S.; Castro, K. A. D. F.; Crotti, A. E. M.; Calefi, P. S.; Nassar, E. J.; Ciuffi, K. J.; *Appl. Catal., A* **2010**, *389*, 147.
38. Cestari, A.; Bandeira, L. C.; Calefi, P. S.; Nassar, E. J.; Ciuffi, K. J.; *J. Alloys Compd.* **2009**, *472*, 299.
39. Cestari, A.; Ávila, L. R.; Nassor, E. C. O.; Pereira, P. F. S.; Calefi, P. S.; Ciuffi, K. J.; Nakagaki, S.; Gomes, A. C. P.; Nassar, E. J.; *Mater. Res.* **2009**, *12*, 139.
40. Ciuffi, K. J.; Caetano, B. L.; Rocha, L. A.; Molina, E. F.; Rocha, Z. N.; Ricci, G. P.; de Lima, O. J.; Calefi, P. S.; Nassar, E. J.; *Appl. Catal., A* **2006**, *311*, 122.
41. Ciuffi, K. J.; de Lima, O. J.; Sacco, H. C.; Nassar, E. J.; *J. Non-Cryst. Solids* **2002**, *304*, 126.
42. de Lima, O. J.; Sacco, H. C.; Oliveira, D. C.; Aguirre, D. P.; Silva, M. A.; Mello, C.; Leite, C. A. P.; Ciuffi, K. J.; *J. Mater. Chem*. **2001**, *11*, 2476.
43. Nassar, E. J.; Ciuffi, K. J.; Calefi, P. S.; Ávila, L. R.; Bandeira, L. C.; Cestari, A.; de Faria, E. H.; Marçal, A. L.; Matos, M. G. In *Europium: Compounds, Production and Applications*; Wright, H. K.; Edwards, G. V., eds.; Nova Science Publishers: Hauppauge, 2010, ch. 1.
44. Acosta, S.; Corriu, R. J. P.; Leclercq, D.; Lefèvre, P.; Mutin, P. H.; Vioux, A.; *J. Non-Cryst. Solids* **1994**, *170*, 234.
45. Wright, J. D.; Sommerdijk, N. A. M.; *Sol-Gel Materials: Chemistry and Applications*, 1st ed.; Gordon and Breach Science Publishers: Amsterdam, 2001.
46. Brinker, C. J.; Scherer, G. W.; *Sol-Gel Science: the Physics and Chemistry of Sol-Gel Processing*; Academic Press: San Diego, 1990.

47. Aegerter, M. A.; Menning, M.; *Sol-Gel Technologies for Glass Producers and Users*; Kluwer Academic Publishers: Boston, 2004.
48. Hay, J. N.; Raval, H. M.; *Chem. Mater*. **2001**, *13*, 3396.
49. Ribeiro, G. S.; Prado, R. J.; *Quim. Nova* **2010**, *33*, 1104.
50. Patra, A.; Tallman, R. E.; Weinstein, B. A.; *Opt. Mater.* **2005**, *27*, 1396.
51. Powell, R. C.; *Physics of Solid State Laser Materials*; Springer: New York, 1998.
52. Mi, X.; Zhang, X.; Ba, X.; Bai, Z.; Lu, L.; Wang, X.; Liu, Q.; *Adv. Powder Technol.* **2009**, *20*, 164.
53. Jamison, S. P.; Imbusch, G. F.; *J. Lumin.* **1997**, *75*, 143.
54. Yang, Z.; Lin, Y. S.; *J. Ind. Eng. Chem.* **2000**, *39*, 4944.
55. Lee, D.; Takahashi, H.; Thankamony, A. S. L.; Dacquin, J. P.; Bardet, M.; Lafon, O.; De Paëpe, G.; *J. Am. Chem. Soc.* **2012**, *134*, 18491.
56. Andonova, S.; Vladov, Ch.; Pawelec, B.; Shtereva, I.; Tyuliev, G.; Damyanova, S.; Petrov, L.; *Appl. Catal., A* **2007**, *328*, 201.
57. Tanabe, Y.; Sugano, S.; *J. Phys. Soc. Jpn.* **1954**, *9*, 753.
58. Sosman, L. P.; da Fonseca, R. J. M.; Tavares Jr., A. D.; Barthem, R. B.; Abritta, T.; *Rev. Mater*. **2007**, *12*, 276.
59. Costa, V. C.; Lameiras, F. S.; Pinheiro, M. V. B.; Sousa, D. F.; Nunes, L. A. O.; Shen, R.; Bray, K. L.; *J. Non-Cryst. Solids* **2000**, *273*, 209.
60. Boyrivent, A.; Duval, E.; *J. Phys. C: Solid State Phys*. **1978**, *11*, 439.
61. Bondzior, B.; Miniajluk, N.; Deren, P. J.; *Opt. Mater.* **2018**, *79*, 269.
62. Williams, Q.; Jeanloz, R.; *Phys. Rev. B: Condens. Matter Mater. Phys.* **1985**, *31*, 7449.
63. Williams, Q.; *J. Phys. Chem. Solids* **2017**, *109*, 89.

Submitted: June 28, 2018
Published online: October 2, 2018